Hindawi Publishing Corporation
Journal of Nanomaterials
Volume 2013, Article ID 367510, 8 pages
http://dx.doi.org/10.1155/2013/367510

Research Article

Preparation of Smooth Surface TiO_2 Photoanode for High Energy Conversion Efficiency in Dye-Sensitized Solar Cells

Sasipriya Kathirvel,[1] Huei-Siou Chen,[1] Chaochin Su,[1] Hsiue-Hsyan Wang,[1] Chung-Yen Li,[2] and Wen-Ren Li[2]

[1] *Institute of Organic and Polymeric Materials, National Taipei University of Technology, Taipei 10608, Taiwan*
[2] *Department of Chemistry, National Central University, Chung-Li 32001, Taiwan*

Correspondence should be addressed to Chaochin Su; f10913@ntut.edu.tw and Wen-Ren Li; ch01@ncu.edu.tw

Received 14 December 2012; Accepted 2 April 2013

Academic Editor: Wen Zeng

Dye-sensitized solar cells (DSSCs) based on a TiO_2 photoanode have been considered as an alternative source in the field of renewable energy resources. In DSSCs, photoanode plays a key role to achieve excellent photo-to-electric conversion efficiency. The surface morphology, surface area, TiO_2 crystal phase, and the dispersion of TiO_2 nanoparticles are the most important factors influencing the properties of a photoanode. The smooth TiO_2 surface morphology of the photoanode indicates closely packed arrangement of TiO_2 particles which enhance the light harvesting efficiency of the cell. In this paper, a smooth TiO_2 photoanode has been successfully prepared using a well-dispersed anatase TiO_2 nanosol *via* a simple hydrothermal process. The above TiO_2 photoanode was then compared with the photoanode made from commercial TiO_2 nanoparticle pastes. The morphological and structural analyses of both the aforementioned photoanodes were comprehensively characterized by scanning electron microscopy and X-ray diffraction analysis. The DSSC fabricated by using a-TiO_2 nanosol-based photoelectrode exhibited an overall light conversion efficiency of 7.20% and a short-circuit current density of 13.34 mA cm^{-2}, which was significantly higher than those of the DSSCs with the TiO_2 nanoparticles-based electrodes.

1. Introduction

Much interest has been focused on the development of dye-sensitized solar cell (DSSC) technology, due to its low cost and easy fabrication with excellent photo-to-electric conversion efficiency [1–5]. Recently, the maximum photo-to-electric conversion efficiency of DSSCs was reported to exceed 13% at 509 W/m^2 simulated solar intensity [5]. Even though DSSCs have their unique advantages, further improving the efficiency is still a key challenge [6–8]. The DSSCs were composed of a photoanode, a sensitizer, a redox-coupled electrolyte, and a counter electrode [9]. Among them, the photoanode is the main component in DSSC and it significantly influences the photo-to-electric conversion efficiency of the cell, due to its dye loading, electron transportation, and electron collection characteristics [10, 11]. The photogenerated electron transport and collection are slow in the nanoparticles-based photoanode due to the recombination of electrons [7, 12]. Hence, a well performing photoanode with desirable properties, such as high surface area, smooth surface morphology with less grain boundaries for fast electron transport, is essential for the development of a high performance solar cell [13–15].

The nanocrystalline TiO_2 film is one of the most commonly employed photoanode materials in DSSCs due to its excellent optoelectronic properties [16]. TiO_2 nanomaterials mainly exist as anatase, rutile, and brookite crystalline phase and anatase TiO_2 phase has been mostly utilized in DSSCs application [17]. Even though the rutile TiO_2 is thermodynamically stable, it possesses a smaller surface area, larger crystallite size, and lower Fermi energy level, compared to anatase TiO_2 [18, 19]. The surface morphology, particle size, surface area, porosity, crystalline phase, and dispersion of TiO_2 nanoparticles are the various influencing factors which determine the performance of a photoanode [20–22]. For instance, Park et al. investigated the effect of both

base-treated and acid-treated TiO_2 to analyze the effect of particle size, shape, film porosity, and surface structure on the performance of DSSCs [23]. For a typical photoanode, TiO_2 nanoparticle film with a thickness of 12–14 μm was utilized for highly efficient DSSCs [9]. So far, TiO_2 nanoparticle films were fabricated using the pastes prepared from TiO_2 nanopowders. Ito et al. have studied the homogenization effect of a different TiO_2 pastes by dispersing TiO_2 powders *via* both ball-milling and mortar-grinding route, in which the monodispersed particles were obtained by the former process [24]. Lee et al. studied the influence of the surface morphology of the TiO_2 film on the performance of DSSC, in which the TiO_2 paste was prepared using a poly(ethylene glycol) binder [25]. Dhungel and Park fabricated DSSCs using different TiO_2 pastes by varying the proportion of nanocrystalline particles of TiO_2 with particle size distribution in a wide range [26]. The TiO_2 film morphology, interparticle interaction, and the connection between the TiO_2 film and conductive substrate are essential for the better dye adsorption and transportation of electrons to the counter electrode with reduced charge recombination. Hence, it is very important to prepare the TiO_2 film with highly dispersed TiO_2 nanoparticles. The preparation of unagglomerated TiO_2 paste from the homogeneous TiO_2 suspension is one of the approaches to obtain a desired TiO_2 film. Jeong et al. used a TiO_2 colloidal suspension to prepare an α-terpineol-based TiO_2 paste and compared with the commercial dyesol TiO_2 paste [27]. Based on the above considerations, in order to obtain an effective TiO_2 photoanode, the preparation of different types of TiO_2 pastes using the TiO_2 nanosol and TiO_2 nanopowders was carried out.

In the present investigation, the TiO_2 nanosol was prepared by hydrothermal process using titanium (Ti) precursor and its effect on the performance of DSSCs was evaluated. The TiO_2 nanosol-based pastes were compared with the TiO_2 nanopowders-based pastes. The photovoltaic performance indicated that the anatase TiO_2 nanosol-based photoelectrode exhibited higher photocurrent density and higher efficiency than that of the photoelectrode using TiO_2 nanoparticles. This result may be attributed to the large amount of dye adsorption on the TiO_2 nanosol which has higher surface area with highly dispersed uniform a-TiO_2 particles.

2. Experimental Procedure

2.1. Materials. Titanium (IV) n-butoxide (TnB, 99%, ACROS) and acetic acid (99.8%, Scharlau, analytical grade), were used for the synthesis of TiO_2. P25 (Degussa, Germany), ST-01 (Ishihara Sangyo, Japan), and ST-21 (Ishihara Sangyo, Japan) commercial TiO_2 nanoparticles were used for the comparison analysis. Ethyl cellulose (45 cp and 10 cp) and α-terpineol were used for the preparation of TiO_2 pastes.

2.2. Preparation of TiO_2 Nanosol. Titanium (IV) n-butoxide was added slowly into the acetic acid (2 M) solution. The solution was stirred for 4-5 days until obtaining a translucent white solution. Then, the mixture was hydrothermally treated at 200°C for 5 h. The obtained white precipitate solution was cooled to room temperature, centrifuged, and washed once with distilled (DI) water and twice with ethanol. The centrifuged white precipitate was dispersed into 40 mL of anhydrous ethanol and kept stirring for one day. Subsequently, the centrifuged white precipitate was dispersed into 40 mL of anhydrous ethanol and kept stirring for one day. This sample is hereafter named as anatase TiO_2 (a-TiO_2) nanosol (NS) because of its anatase crystal phase.

2.3. Preparation of a-TiO_2 Nanosol-Based Paste. To prepare a-TiO_2 nanosol-based paste, the obtained precipitate after hydrothermal treatment was centrifuged/washed and dispersed into anhydrous ethanol under stirring for 24 h and sonicated further for proper homogeneous dispersion. Then, 25.96 g of α-terpineol and the mixture solution of two viscosities of ethyl cellulose (10 cp-1.8 g and 45 cp-1.4 g) in anhydrous ethanol (29 g) were added into the above solution, followed by repeated sonication for three times. The above solution was evaporated using the rotary evaporator at 40°C until to obtain a viscous paste. Finally, the paste was rolled using three-roller miller.

2.4. Preparation of TiO_2 Nanoparticles-Based Paste. Little modifications were carried out for the preparation of TiO_2 paste using TiO_2 nanoparticles, namely, P-25, ST-01, and ST-21. Briefly, 6 gram of TiO_2 nanoparticles was dispersed into the mixture of DI water, acetic acid, and anhydrous ethanol. Then the mixture was kept stirring for 24 h and sonicated for 5 min. Furthermore, the solution was sonicated 5 min followed by the addition of α-terpineol and again sonicated for 5 min after adding ethyl cellulose. The remaining procedure is the same as mentioned above in the preparation of TiO_2 nanosol paste.

2.5. Preparation of TiO_2 Photoanode and Solar Cell Assembly. Fluorine doped tin oxide (FTO, Solaronix, 8 Ωcm^{-2}) conducting glass was cleaned in detergent liquid, distilled water, acetone and methanol using an ultrasonic bath each for 30 min. Then the TiO_2 paste was screen printed (Screen Printing Machine, Weger, WE-400F, Guger Industries Co., Ltd.) on cleaned FTO substrate and dried at 110°C. The process was repeated until to achieve 6 μm thick TiO_2 layer. The TiO_2 films were annealed with a programmable heating process: at 110°C for 30 min, 125°C for 15 min, 325°C for 5 min, 375°C for 5 min, 450°C for 15 min, and 500°C for 15 min. The working area of the TiO_2 films was 0.16 cm^2. The TiO_2 electrodes were cooled to 80°C and then immersed in 0.3 mM N719 dye in acetonitrile/*tert*-butyl alcohol (1 : 1) for 36 h. The sensitized photoanodes and the platinum (Pt, 20 nm, ion beam sputtering E-105) sputtered FTO substrates were sandwiched together using 60 μm surlyn spacers. The ionic electrolyte consisting lithium iodide, iodide, and 4-tert-butylpyridine in acetonitrile was introduced into the hole predrilled on the counter electrode. Finally the hole was sealed using 30 μm surlyn and cover glass.

2.6. Characterization of Samples and Device. The particle size and the morphology of the TiO_2 nanoparticles were analyzed by transmission electron microscopy (TEM, Hitachi, H-7100). The surface morphology of TiO_2 films was studied by scanning electron microscopy (SEM, Hitachi, S-4800). X-ray diffraction (XRD, Rigaku PANalytical X'Pert PRO) measurement was carried out with Cu Kα radiation. The surface area analysis of the TiO_2 nanoparticles was obtained using Brunauer-Emmett-Teller (BET, Micromeritics, Gemini V, ASAP-2010) surface area analyzer, in which all the samples were degassed prior to analyzes. The reflectance UV-visible spectrum was obtained using a Shimadzu UV-3600 spectrometer with an integrating sphere. The amount of adsorbed dye was determined by desorbing the dye from a-TiO_2 surface into a solution of 0.1 M NaOH. The concentration of the adsorbed dye was analyzed by UV-visible spectrophotometer (JASCO, V-630). The current-voltage (*I-V*) characteristics of the cell under one sun irradiation (AM 1.5 filter-Oriel, #81094) using solar simulator with 300 W Xenon lamp (Oriel #91160) were obtained by applying external bias to the cell, and the generated photocurrent was measured by a Keithley model 2400 digital source meter. The incident photon-to-current efficiency (IPCE) was obtained by Model SR830 DSP Lock-In Amplifier and a Model SR540 Optical Chopper (Stanford Research Corporation, USA), a 150 W Xenon lamp and power supply (Oriel, #66902), and a monochromator (Oriel CornerstoneTM 130).

3. Results and Discussions

3.1. Structural Characterization of TiO_2 Nanoparticles and TiO_2 Films. The anatase TiO_2 (a-TiO_2) nanosol prepared by hydrothermal process was used to prepare TiO_2 paste (nanosol-based TiO_2 paste). The commercially available TiO_2 nanoparticles (P-25, ST-01, and ST-21) were concomitantly utilized to prepare TiO_2 pastes (nanoparticle-based TiO_2 pastes) by similar procedure (Section 2.4). Both types of TiO_2 pastes were screen-printed on FTO substrate and annealed with stepwise heating process in order to compare the effect of TiO_2 photoanodes prepared from nanosol-based TiO_2 paste and nanoparticle-based TiO_2 pastes in DSSCs. Figure 1 shows the typical SEM photographs of nanosol-based TiO_2 film (NS film) and nanoparticle-based TiO_2 films (P-25 film, ST-01 film, and ST-21 film) with two kinds of magnifications. The noteworthy difference in the morphology of NS film (Figure 1(a)) and nanoparticle-based TiO_2 films (Figures 1(b)–1(d)) could be observed instantaneously from the SEM images with lower magnifications (×5,000). The NS film (Figure 1(a)) is extremely smooth and uniform. This result indicates that the highly dense TiO_2 particles formed are homogeneously dispersed throughout the NS film.

It can be further confirmed by the higher resolution SEM image (Figure 1(e), ×50,000). Comparatively, all the nanoparticle-based TiO_2 films show rough surface morphology which is evident in the higher magnification images (Figures 1(f)–1(h)). For P-25 film (Figures 1(b) and 1(f)), some voids between the closely packed TiO_2 nanoparticles were observed on the porous TiO_2 layers. The ST-21 film (Figures 1(d) and 1(h)) surface is rough with TiO_2 aggregates of about 300 nm. In the case of ST-01 film, a completely clumpy and nonuniform surface morphology was observed. The clumpy structure is formed by aggregation of TiO_2 particles of size from submicron to several microns. The observation of individual TiO_2 nanoparticles is hardly distinguishable.

This result is consistent with the surface-profiling measurement (results not shown here) in which the screen printed TiO_2 film made from nanosol-based TiO_2 paste is relatively flat compared with that made from nanoparticle-based TiO_2 pastes. For comparison, the thickness of TiO_2 films from nanosol-based TiO_2 paste and nanoparticle-based TiO_2 pastes were all controlled at about 6 μm.

It is concluded from the aforementioned SEM analysis that the nanosol-based TiO_2 electrode reveals smoother surface morphology characteristics in comparison with the nanoparticle-based TiO_2 electrodes. This can be insight by investigation of the size and surface morphology of TiO_2 nanoparticles. Figure 2 shows the TEM micrographs of (a) TiO_2 nanosol, (b) P-25, (c) ST-01, and (d) ST-21 samples. The TiO_2 particles in TiO_2 nanosol are well-dispersed irregular polyhedron which is typical for anatase phase TiO_2. Similar TEM morphologies are observed for commercial TiO_2 nanoparticles except for ST-01, where severe agglomeration occurs presumably due to the extremely small TiO_2 particle size. The average particle size of P-25, ST-01, and ST-21 samples is ~35 nm, 5 nm, and 27 nm, respectively. The size of TiO_2 nanoparticles (TiO_2-NP, TEM not shown) worked out (just drying) from TiO_2 nanosol is ~20 nm. The particle size of TiO_2 can also be estimated from BET surface area measurement. The TiO_2-NP, P-25, ST-01, and ST-21 nanoparticles possess specific surface area of 108.5, 51.6, 247.9, and 65.1 m^2/g, respectively, which is consistent with the TEM size measurement. The results of TiO_2 particle size calculated from TEM and BET are also summarized in Table 1 and compared with the crystalline size obtained from XRD.

The TEM particle size analysis was also performed for TiO_2 samples after sintering at 500°C in order to imitate the annealing process after screen-printing the TiO_2 pastes onto FTO substrate. The particle size is marginally enlarged. The average particle size of TiO_2-NP, P-25, ST-01, and ST-21 samples after sintering is ~35 nm, 42 nm, 27 nm, and 39 nm, respectively (Table 1).

Consistent with TEM analysis, the surface area from BET measurement decreased to 82.3, 51.3, 99.5, and 58.6 m^2/g. The ST-01 TiO_2 is more dispersed. It is expected that the growth of TiO_2 nanoparticles upon high temperature heat treatment may lead to the clumpy surface morphology of TiO_2 electrodes as seen from SEM images (Figure 1) for P-25 film, ST-01 film, and ST-21 film. As for the NS-film, the as-synthesized TiO_2 nanoparticles in a-TiO_2 nanosol were evenly well dispersed with unique morphological configuration on FTO. Although the heat-induced aggregation may occur to some extent after annealing, it does not significantly affect the surface morphology. Both TEM characterization and BET analysis reveal that the utilization of TiO_2 nanosol is more desirable than the TiO_2 nanoparticles for the fabrication of TiO_2 films.

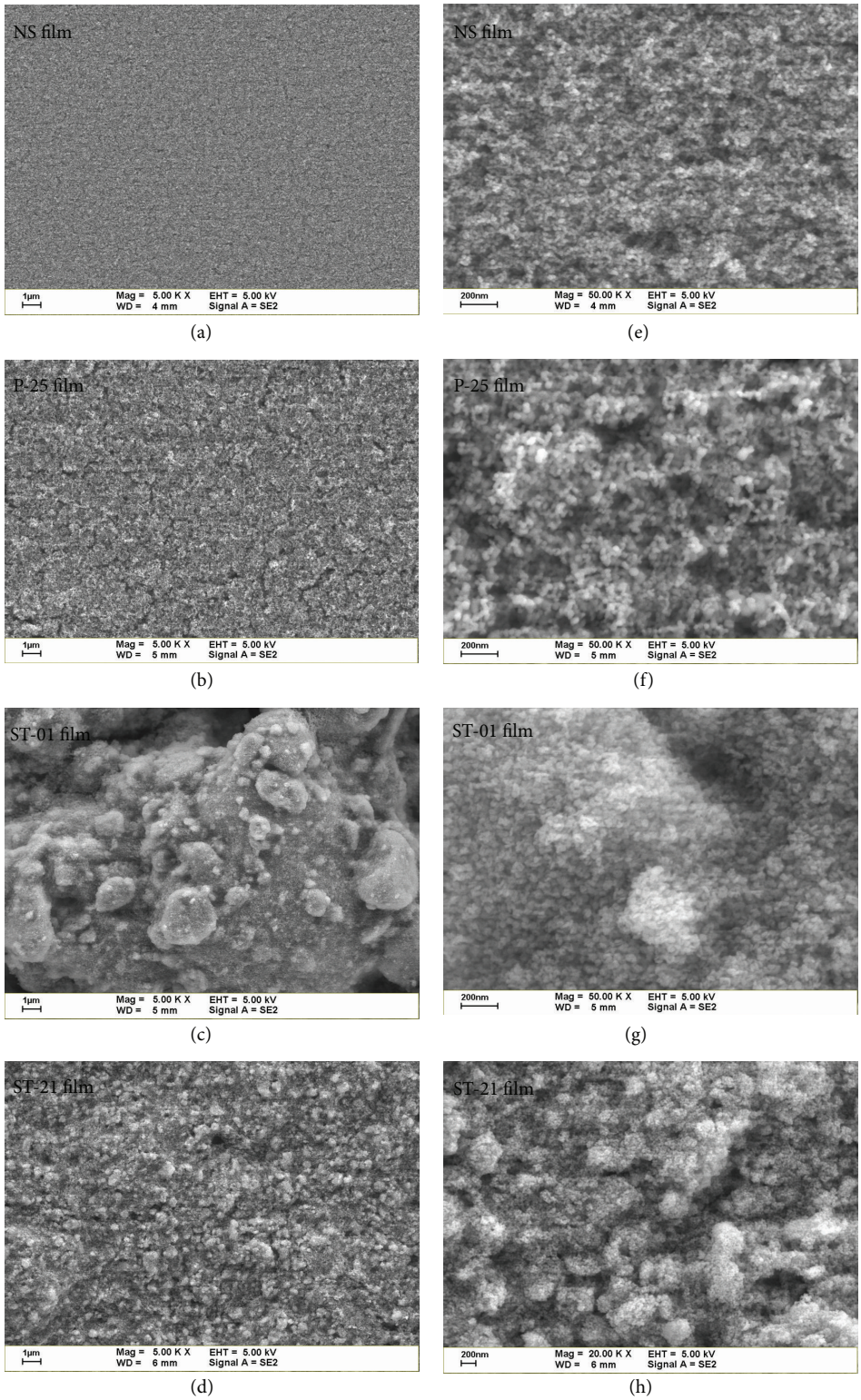

Figure 1: SEM images of (a) a-TiO_2 nansol film, (b) P-25 TiO_2 film, (c) ST-01 film, and (d) ST-21 film, ((e), (f), (g), and (h)) SEM images at higher magnification (×20,000) of samples (a), (b), (c), and (d), respectively.

Table 1: Crystallite size, particle size, and specific surface area of various TiO_2 nanoparticles.

Sample	Crystallite size (nm) *film	Particle size (nm) (before sintering) TEM	Particle size (nm) (after sintering) TEM	BET (m^2/g) (before sintering)	BET (m^2/g) (after sintering)
TiO_2-NP	20	20 (NS)	35	108.5	82.3
P-25	21 (anatase) 70 (rutile)	35	42	51.6	51.3
ST-01	7	5	27	247.9	99.5
ST-21	21	27	39	65.1	58.6

*Represents for film, NS indicates for TiO_2 nanosol.

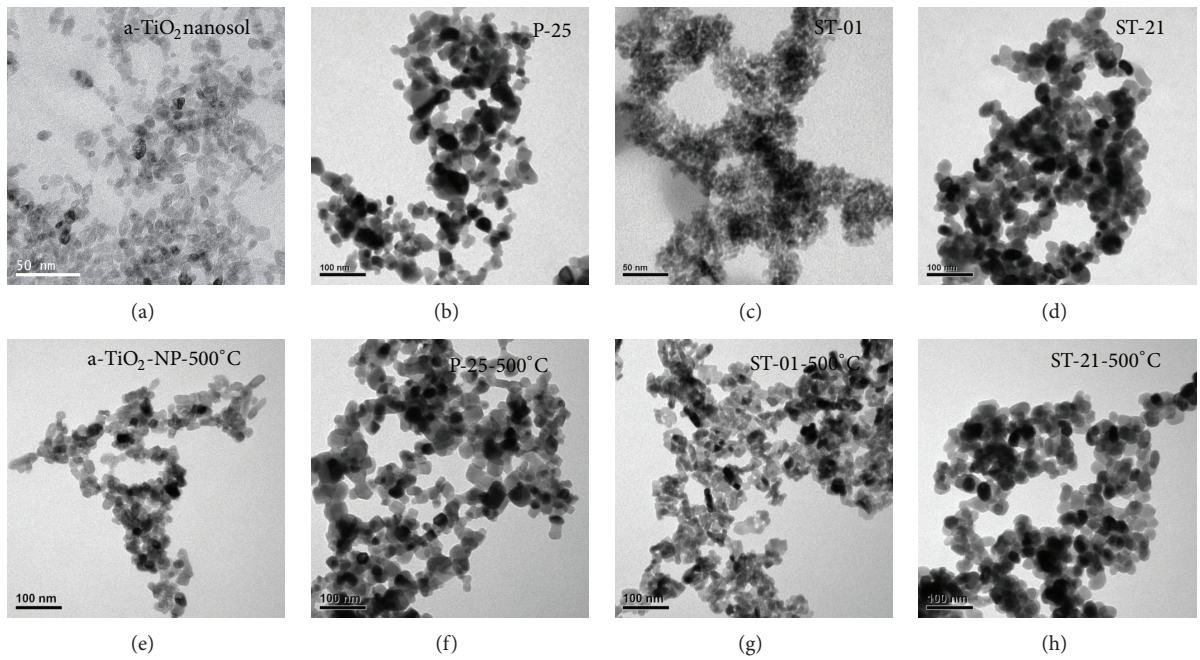

Figure 2: TEM image (a) a-TiO_2 nanosol (b) P-25, (c) ST-01, (d) ST-21 ((a)–(d)) before sintering ((e)–(h)) after sintering at 500°C.

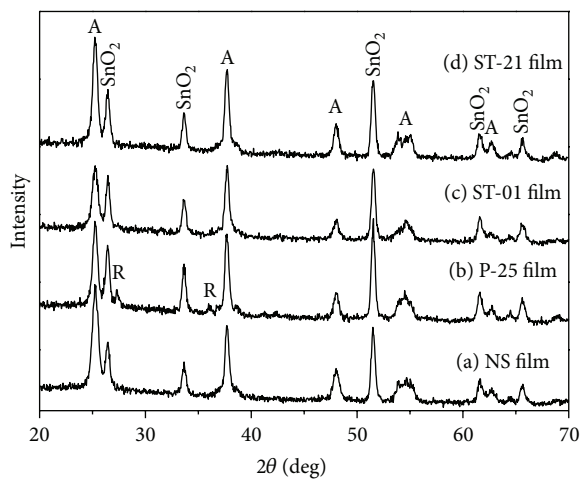

A: Anatase
R: Rutile

Figure 3: XRD pattern of various TiO_2 electrodes.

The crystal phase of TiO_2 films was determined by XRD. Figure 3 illustrates the XRD patterns of (a) NS films, (b) P-25 film, (c) ST-01 film, and (d) ST-21 film deposited on FTO substrate. The XRD patterns mainly indexed to anatase phase (A: anatase) with diffraction angle of 2θ at 25.23°, 37.67°, 48.05°, 53.90°, 55.03°, and 62.68° corresponding to the characteristic anatase peaks. Several peaks appearing at 26.6°, 33.9°, and 51.8° in Figure 3 are due to the SnO_2 from FTO substrate. These results indicate that the TiO_2 films exhibit a stable anatase phase even after annealing at higher temperature of 500°C. No phase transformation was detected. Only P-25 film shows some rutile (R: rutile) characteristics diffraction peaks corresponding to about 20% of rutile TiO_2. This is consistent with the crystal phase of original P-25 TiO_2 nanoparticles (XRD not shown). The average crystallite size of NS film, P-25 film, ST-01 film, and ST-21 film was estimated from the (101) peak according to the Scherrer equation, $D = 0.89\lambda/\beta\cos\theta$, where λ, β, and θ refer to X-ray wavelength (nm), the full width at half-maximum, and the diffraction

Table 2: Photovoltaic properties of the DSSCs made from a-TiO_2 sol and commercial DP-25, ST-01, and ST-21 TiO_2 photoanode.

DSSCs	Thickness (μm)	$N719_{ads}$ (μmol/cm^2)	J_{sc} (mA/cm^2)	V_{oc} (V)	FF	η (%)
NS cell	6	0.132	13.34	0.77	0.70	7.20
P-25 cell	6	0.088	10.76	0.79	0.71	6.04
ST-01 cell	6	0.110	9.45	0.79	0.74	5.53
ST-21 cell	6	0.092	10.96	0.80	0.70	6.21

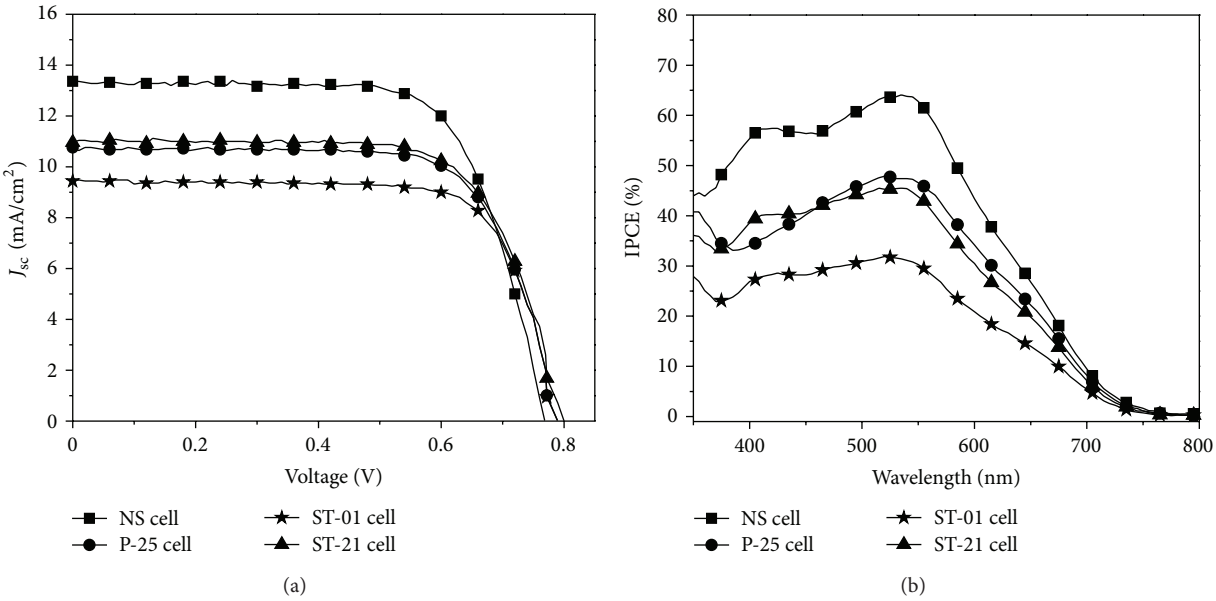

Figure 4: (a) Current-voltage curve (b) Incident photon-to-current conversion efficiency (IPCE) curves of various TiO_2 photoelectrodes.

angle, respectively. The crystallite sizes listed in Table 1 are in good agreement with the TEM data.

3.2. Photovoltaic Properties. The photovoltaic performance of DSSCs (NS cell, P-25 cell, ST-01 cell, and ST-21 cell) fabricated using the above prepared TiO_2 photoelectrodes (NS film, P-25 film, ST-01 film, and ST-21 film) was characterized by evaluating the current-voltage behaviour under one sun AM 1.5 irradiation from a solar simulator. Figure 4(a) shows the photocurrent-voltage characteristics (*I-V*) curves. Table 2 summarizes the TiO_2 film thickness, the amount of dye adsorption ($N719_{ads}$), and the photoelectric data of the DSSCs in Figure 4(a), including, the short-circuit photocurrent density (J_{sc}), an open circuit voltage (V_{oc}), fill factor (FF), and photo-to-electric conversion efficiency (η). It is apparent that the a-TiO_2 nanosol based photoelectrode achieved the highest photo-to-electric conversion efficiency of 7.20% with a short circuit current density of 13.3 mA/cm^2, $N719_{ads}$ of 0.132 μmol/cm^2, V_{oc} of 0.77 V, and FF of 0.70. In contrast to the DSSCs made from TiO_2 nanoparticle-based photoelectrode, the photo-to-electric conversion performance was significantly enhanced by using the TiO_2 nanosol-based photoelectrode. The efficiency and short-circuit current density of DSSCs are mainly affected by the dye adsorption on the TiO_2 electrode. As expected, from the SEM analysis, the amount of dye adsorbed on TiO_2 nanosol based-photoelectrode was higher than that on the TiO_2 nanoparticles-based photoelectrodes (Table 2).

Even though, the dye adsorption is higher for ST-01 nanoparticle based-photoelectrode than P-25 and ST-21 photoelectrode, the J_{sc} (mA/cm^2) and η (%) are lower. This might be attributed to the large aggregation of the TiO_2 nanoparticles. Inhomogeneous film configuration creates electron traps that hinders the electron transportation and leads to the lower DSSCs efficiency. The TiO_2 nanosol-based photoelectrode exhibits 19%, 30%, and 16% increase in the photo-to-electric conversion efficiency compared to the P-25, ST-01, and ST-21 photoelectrode, respectively.

Higher photo-to-electric conversion efficiency and short-circuit density of a-TiO_2 nanosol-based photoelectrode are attributed to higher amount of dye adsorption owing to larger surface area and more compact smooth surface morphology of TiO_2 photoanode. The higher dye adsorption value reveals that a-TiO_2 nanosol-based paste is well interconnected and the electrons are efficiently transported through the film which is consistent with the work reported by Jeong et al. [27]. The incident photon-to-current conversion efficiency (IPCE) spectra were further measured for the above prepared DSSCs. From Figure 4(b), we can observe that the IPCE% efficiency for all the samples was maximum at the wavelength of 550 nm. Again, the NS cell shows a significant increase

in IPCE percentage value over the long-wavelength range (530–700 nm) compared with other cells made from TiO_2 nanoparticles. This improvement in the long-wavelength range could be attributed to the enhancement of dye adsorption of the smooth TiO_2 film surface, leading to higher J_{sc}. Further studies are required to analyze the properties of charge transport and electron recombination process in DSSCs.

4. Conclusion

The present work has demonstrated the effect of a-TiO_2 nanosol on the performance of DSSCs in comparison with the TiO_2 nanoparticles. The well dispersed oval shaped a-TiO_2 nanosol-based TiO_2 film (6 μm thickness) with larger surface area results in higher dye adsorption, compared to the commercial TiO_2 nanoparticles film. Hence, a-TiO_2 nanosol-based photoanode exhibits a short-circuit current density (J_{sc}) of 13.3 mA cm^{-2}, an open-circuit voltage (V_{oc}) of 0.77 V, and a fill factor (FF) of 0.70 and achieves an overall light conversion efficiency (η) of 7.2%. The performance of the above photoelectrode was significantly higher than the commercial P-25, ST-01, and ST-21 nanoparticle-based electrodes, owing to the higher dye loading. In addition, the NS cell shows higher IPCE efficiency than that of TiO_2 nanoparticles based DSSCs.

Authors' Contribution

S. Kathirvel and Huei-Siou Chen have equally contributed.

Acknowledgments

The authors gratefully acknowledge the National Science Council of Taiwan (Project no. NSC 98-2113-M-027-003-MY3 and 100-2113-M-008-004-MY3) for the financial support to carry out this research project.

References

[1] B. O'Regan and M. Grätzel, "A low-cost, high-efficiency solar cell based on dye-sensitized colloidal TiO_2 films," *Nature*, vol. 353, no. 6346, pp. 737–740, 1991.

[2] M. Grätzel, "Photoelectrochemical cells," *Nature*, vol. 414, no. 6861, pp. 338–344, 2001.

[3] A. Hagfeldt, G. Boschloo, L. Sun, L. Kloo, and H. Pettersson, "Dye-sensitized solar cells," *Chemical Reviews*, vol. 110, no. 11, pp. 6595–6663, 2010.

[4] J. Nelson and R. E. Chandler, "Random walk models of charge transfer and transport in dye sensitized systems," *Coordination Chemistry Reviews*, vol. 248, no. 13-14, pp. 1181–1194, 2004.

[5] A. Yella, H.-W. Lee, H. N. Tsao et al., "Porphyrin-sensitized solar cells with cobalt (II/III)-based redox electrolyte exceed 12 percent efficiency," *Science*, vol. 334, no. 6056, pp. 629–634, 2011.

[6] M. Grätzel, "Conversion of sunlight to electric power by nanocrystalline dye-sensitized solar cells," *Journal of Photochemistry and Photobiology A*, vol. 164, no. 1–3, pp. 3–14, 2004.

[7] B. E. Hardin, H. J. Snaith, and M. D. McGehee, "The renaissance of dye-sensitized solar cells," *Nature Photonics*, vol. 6, no. 3, pp. 162–169, 2012.

[8] Y.-D. Zhang, X.-M. Huang, D.-M. Li, Y.-H. Luo, and Q.-B. Meng, "How to improve the performance of dye-sensitized solar cell modules by light collection," *Solar Energy Materials and Solar Cells*, vol. 98, pp. 417–423, 2012.

[9] T. W. Hamann, R. A. Jensen, A. B. F. Martinson, H. Van Ryswyk, and J. T. Hupp, "Advancing beyond current generation dye-sensitized solar cells," *Energy and Environmental Science*, vol. 1, no. 1, pp. 66–78, 2008.

[10] J. van de Lagemaat, N. G. Park, and A. J. Frank, "Influence of electrical potential distribution, charge transport, and recombination on the photopotential and photocurrent conversion efficiency of dye-sensitized nanocrystalline TiO_2 solar cells: a study by electrical impedance and optical modulation techniques," *Journal of Physical Chemistry B*, vol. 104, no. 9, pp. 2044–2052, 2000.

[11] L. Vesce, R. Riccitelli, G. Soscia, T. M. Brown, A. Di Carlo, and A. Reale, "Optimization of nanostructured titania photoanodes for dye-sensitized solar cells: study and experimentation of $TiCl_4$ treatment," *Journal of Non-Crystalline Solids*, vol. 356, no. 37–40, pp. 1958–1961, 2010.

[12] A. B. F. Martinson, J. W. Elam, J. Liu, M. J. Pellin, T. J. Marks, and J. T. Hupp, "Radial electron collection in dye-sensitized solar cells," *Nano Letters*, vol. 8, no. 9, pp. 2862–2866, 2008.

[13] U. Opara Krašovec, M. Berginc, M. Hočevar, and M. Topič, "Unique TiO_2 paste for high efficiency dye-sensitized solar cells," *Solar Energy Materials and Solar Cells*, vol. 93, no. 3, pp. 379–381, 2009.

[14] H. Xu, X. Tao, D. T. Wang, Y. Z. Zheng, and J. F. Chen, "Enhanced efficiency in dye-sensitized solar cells based on TiO_2 nanocrystal/nanotube double-layered films," *Electrochimica Acta*, vol. 55, no. 7, pp. 2280–2285, 2010.

[15] Q. Zhang and G. Cao, "Nanostructured photoelectrodes for dye-sensitized solar cells," *Nano Today*, vol. 6, no. 1, pp. 91–109, 2011.

[16] Y. Duan, N. Fu, Q. Liu et al., "Sn-doped TiO_2 photoanode for dye-sensitized solar cells," *The Journal of Physical Chemistry C*, vol. 116, no. 16, pp. 8888–8893, 2012.

[17] I. C. Baek, M. Vithal, J. A. Chang et al., "Facile preparation of large aspect ratio ellipsoidal anatase TiO_2 nanoparticles and their application to dye-sensitized solar cell," *Electrochemistry Communications*, vol. 11, no. 4, pp. 909–912, 2009.

[18] G. Liu, X. Wang, Z. Chen, H. M. Cheng, and G. Q. Lu, "The role of crystal phase in determining photocatalytic activity of nitrogen doped TiO_2 ," *Journal of Colloid and Interface Science*, vol. 329, no. 2, pp. 331–338, 2009.

[19] M. Lv, D. Zheng, M. Ye et al., "Densely aligned rutile TiO_2 nanorod arrays with high surface area for efficient dye-sensitized solar cells," *Nanoscale*, vol. 4, no. 19, pp. 5872–5879, 2012.

[20] Z.-S. Wang, H. Kawauchi, T. Kashima, and H. Arakawa, "Significant influence of TiO_2 photoelectrode morphology on the energy conversion efficiency of N719 dye-sensitized solar cell," *Coordination Chemistry Reviews*, vol. 248, no. 13-14, pp. 1381–1389, 2004.

[21] K. Suttiponparnit, J. Jiang, M. Sahu, S. Suvachittanont, T. Charinpanitkul, and P. Biswas, "Role of surface area, primary particle size, and crystal phase on titanium dioxide nanoparticle dispersion properties," *Nanoscale Research Letters*, vol. 6, no. 1, pp. 1–8, 2011.

[22] J.-Y. Liao, J.-W. He, H. Xu, D.-B. Kuang, and C.-Y. Su, "Effect of TiO_2 morphology on photovoltaic performance of dye-sensitized solar cells: nanoparticles, nanofibers, hierarchical spheres and ellipsoid spheres," *Journal of Materials Chemistry*, vol. 22, no. 16, pp. 7910–7918, 2012.

[23] D.-W. Park, Y.-K. Choi, K.-J. Hwang et al., "Nanocrystalline TiO_2 films treated with acid and base catalysts for dye-sensitized solar cells," *Advanced Powder Technology*, vol. 22, no. 6, pp. 771–776, 2011.

[24] S. Ito, K. Takahashi, S. I. Yusa, T. Imamura, and K. Tanimoto, "Effects of homogenization scheme of TiO_2 screen-printing paste for dye-sensitized solar cells," *International Journal of Photoenergy*, vol. 2012, Article ID 405642, 7 pages, 2012.

[25] K.-M. Lee, V. Suryanarayanan, and K.-C. Ho, "The influence of surface morphology of TiO_2 coating on the performance of dye-sensitized solar cells," *Solar Energy Materials and Solar Cells*, vol. 90, no. 15, pp. 2398–2404, 2006.

[26] S. K. Dhungel and J. G. Park, "Optimization of paste formulation for TiO_2 nanoparticles with wide range of size distribution for its application in dye sensitized solar cells," *Renewable Energy*, vol. 35, no. 12, pp. 2776–2780, 2010.

[27] N. C. Jeong, O. K. Farha, and J. T. Hupp, "A convenient route to high area, nanoparticulate TiO_2 photoelectrodes suitable for high-efficiency energy conversion in dye-sensitized solar cells," *Langmuir*, vol. 27, no. 5, pp. 1996–1999, 2011.